13th International Symposium on Turbulence and Shear Flow Phenomena (TSFP13)
Montreal, Canada, June 25–28, 2024

TURBULENT IMPINGING JETS ON SMOOTH AND ROUGH PLATES

F. Secchi
Institute of Fluid Mechanics
Karlsruhe Institute of Technology
Karlsruhe, Germany
francesco.secchi@kit.edu

D. Gatti
Institute of Fluid Mechanics
Karlsruhe Institute of Technology
Karlsruhe, Germany
davide.gatti@kit.edu

B. Frohnapfel
Institute of Fluid Mechanics
Karlsruhe Institute of Technology
Karlsruhe, Germany
bettina.frohnapfel@kit.edu

ABSTRACT

Near wall momentum and heat transfer characteristics of turbulent jets impinging on smooth and rough plates are assessed using direct numerical simulations. A jet issues from a fully-developed turbulent pipe flow at $Re = 5300$ (based on the pipe diameter D and mean bulk velocity U_b) and impinges normally onto a plate located $2D$ away from the nozzle. Surface roughness is resolved in the simulations using a body-fitted computational mesh within the framework of a spectral element flow solver. For the considered configuration, surface roughness produces a net effect on integral flow properties only in a limited region of the near-wall flow that develops after jet impingement. The present study investigates the links between near-wall turbulence generation mechanisms and surface roughness effects on momentum and wall-heat transfer.

INTRODUCTION

Impinging jets are commonly adopted as efficient means to augment heat transfer rates between a solid surface and a fluid in confined environments. Most notable applications involve the cooling of jet engine turbine blades and electronic devices. Further enhancements in the design of such devices could yield significant benefits from the economic and environmental perspectives. Consequently, jet impingement has garnered substantial attention in the past, with numerous reviews of existing findings currently available in the literature (Ekkad & Singh, 2021; Jambunathan *et al.*, 1992). Jet impingement produces a complex flow that depends on a rather large number of parameters. Limiting the attention to incompressible flows, the most relevant parameters that determine different functioning regimes of the flow are the nozzle-to-plate distance H and the Reynolds number. In case of circular jets, the latter is typically defined using the mean bulk velocity U_b of the in-flowing jet and the nozzle diameter D. According to several experimental and numerical studies (Jambunathan *et al.*, 1992; Dairay *et al.*, 2015), a configuration of particular interest occurs when $H = 2D$. In fact, for such a configuration and for a wide range of Reynolds numbers, shear-layer instabilities, which occur in the free-shear layer of the jet, interact with the target plate producing a favourable increase in the wall-heat flux. The latter, typically assessed in terms of the mean Nusselt number distribution along the impingement plate, shows the emergence of a local peak away from the stagnation region of the flow.

While existing studies investigate how the wall-heat flux is affected by varying the nozzle-to-plate distance and the Reynolds number, only a few assess the influence that surface roughness has on the flow field. The recent review of Ekkad & Singh (2021) reports most of the available results in this respect. The majority of reported investigations addresses global values of wall-heat transfer increase for specific configurations consisting of arrays of multiple jets and engineered rough surfaces (such as plates covered with dimples or fins). Only a few investigations consider a single circular turbulent jet impinging on plates with homogeneous random surface roughness (Wu *et al.*, 2016; Secchi *et al.*, 2022, 2023) and none of these studies address the effects of surface roughness on the wall-heat transfer. In order to tighten this gap, we present direct numerical simulation (DNS) results of a circular turbulent jet impinging on random surface roughness. The access to the flow details allowed by the DNS approach is used to provide insights on the connection of wall-heat transfer and mean flow field characteristics of impinging jets.

METHODOLOGY

The flow configuration considered in the present study is sketched in figure 1. A jet originates from a fully-developed turbulent pipe flow and impinges orthogonal onto a plate placed at a distance $H = 2D$ away from the jet exit section. The Reynolds number, based on the nozzle diameter D and bulk mean velocity U_b, is $Re = 5300$. For all the simulated cases, the Prandtl number of the fluid is $Pr = 1$. The divergence-free velocity and temperature fields are governed by the incompressible Navier-Stokes equations augmented with a transport diffusion equation for the temperature, which is treated as a passive scalar. Fully-developed inflow boundary conditions are enforced at the inlet section of the computational domain using a precursor simulation of a fully-developed turbulent pipe flow. No-slip velocity boundary conditions are applied on both the impingement and confinement plates, whereas

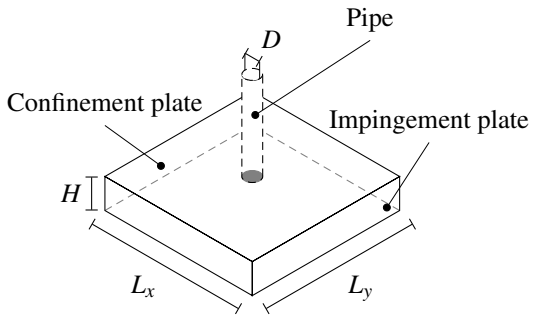

Figure 1. Computational domain and relevant geometrical parameters. The shaded area highlights the inflow section of the computational domain.

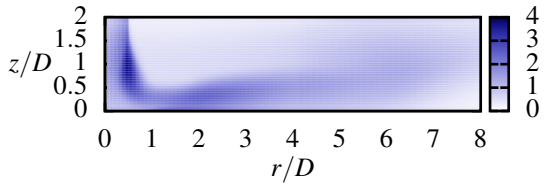

Figure 2. Mesh resolution: color map of the ratio local grid size Δ to Kolmogorov length scale η for the smooth wall case.

the energy-stable open-boundary conditions presented in Dong (2015) and Liu *et al.* (2020) are prescribed on the lateral surfaces of the domain for the velocity and temperature fields respectively. The impingement plate is kept at a constant and uniform temperature T_w and the confinement plate is considered at thermal equilibrium with the incoming jet flow at a temperature $T_j < T_w$.

Within the present numerical framework, the governing equations are recast in weak form according to standard Galerkin formalism and are discretised in space on a Cartesian grid using the spectral element method (Maday & Patera, 1989). Time advancement is performed through an operator splitting procedure coupled with a third-order interpolation-extrapolation time integration scheme in which non-linear terms are treated explicitly and linear terms implicitly. The numerical method is implemented in the open-source flow solver `Nek5000` Fisher *et al.* (2008-2020).

The computational box of the jet flow domain has sizes $L_{x_1} = L_{x_2} = 8D$ in the x_1 and x_2 directions and it is discretised into $156 \times 156 \times 48$ elements in the x_1, x_2, and x_3 directions, respectively. Wall-normal clustering of elements toward the impingement plate is used to better resolve the near-wall region. Stretching of elements is also applied in the x_1 and x_2 directions in order to cluster elements around the stagnation region of the flow. Results reported in this study refer to a 7^{th} polynomial degree solution and, hence, to a computational grid of the jet domain consisting of approximately $598 \cdot 10^6$ grid points. The mesh resolution was checked by comparing the local grid size $\Delta = (\Delta x_1 \Delta x_2 \Delta x_3)^{1/3}$ with the Kolmogorov length scale $\eta = (\nu^3/\varepsilon)^{1/4}$, where Δx_i, $i = 1, 2, 3$ is the local grid spacing along the coordinate direction i, ν is the kinematic viscosity of the fluid and ε is the mean rate of dissipation of turbulent kinetic energy per unit mass. The spatially averaged ratio of local grid size Δ to Kolmogorov length scale η is shown in figure 2 for the smooth wall case. A similar resolution was obtained also for the rough wall case. From the figure, it is observed that $\Delta < 4\eta$ everywhere in the computational domain and that it reaches much lower values in the near wall region. As such, the computational mesh was considered adequate to resolve all relevant scales of turbulent motion.

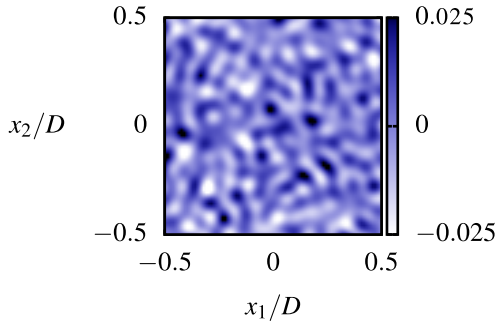

Figure 3. Roughness wall-height color map.

Time averaging was carried out for all the simulated cases for approximately $250D/U_b$. Furthermore, statistical convergence is accelerated by performing averaging along the circumferential direction. Throughout the text, averaging in time is denoted by an over-line $\overline{\cdot}$, whereas averaging in the circumferential direction is indicated by angular brackets $\langle\cdot\rangle$. As a result, the time and space averaged flow field results in a two-dimensional field spanned by the radial distance from the jet axis r and the wall-normal distance $z = x_3$.

Surface roughness is described by a random in-plane wall-height distribution generated using an algorithm presented in Pèrez-Ràfols & Almqvist (2019), which can generate roughness topographies having prescribed power spectrum (PS) and probability density function (PDF). The investigated rough surface has a Gaussian PDF with zero mean value and 99% of the PDF confidence interval of $k_{99} = 0.05D$. Further, the roughness topography is filtered in order to have the shortest resolved wave-length $\lambda_{min} = 0.04D$. A sample of the rough surface is displayed in figure 3. Surface roughness is resolved in the simulations using a body-conforming grid which is obtained by applying a wall-normal deformation to each grid node of the computational domain. In particular, the mesh deformation is maximum for grid nodes lying on the bottom of the computational domain, it decreases linearly with increasing wall-normal distance, and it vanishes for wall-normal distances greater than $x_3 = D$. As a result, the plane of the mean roughness height corresponds to the plane $x_3 = 0$, and the computational domain extends, on average, from $x_3 = 0$ to $x_3 = 2D$.

RESULTS AND OUTLOOK

Jet impingement produces a flow that develops as a wall jet along the impinging plate. This scenario is depicted in figure 4, where a color map of the mean axial velocity $\langle\overline{u_z}\rangle$ distribution is visualized for the smooth wall case. In the figure, mean radial velocity and temperature profiles at different radial locations are used to highlight the development of the flow. A wall jet is characterised by an inner and an outer layer that resemble, respectively, a canonical turbulent boundary layer and a free shear flow.

A measure of the boundary layer thickness is given by the wall-normal height z_m at which the mean radial velocity profile

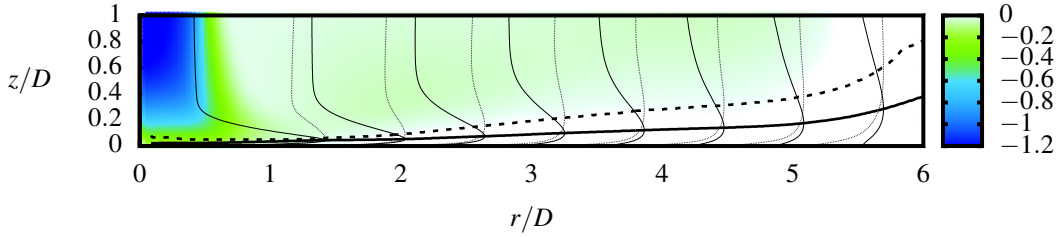

Figure 4. Wall jet development along the impingement plate for the smooth wall case. ———, Velocity boundary layer thickness z_m; - - - - -, temperature boundary layer thickness $z_{\theta,m}$. Solid black thin lines represent mean radial velocity profiles $\langle\overline{u_r}\rangle/U_b$, whereas thin dotted lines represent mean temperature profiles $(T_w - \langle\overline{T}\rangle)/(T_w - T_j)$. The color map displays the mean axial velocity distribution $\langle\overline{u_z}\rangle/U_b$.

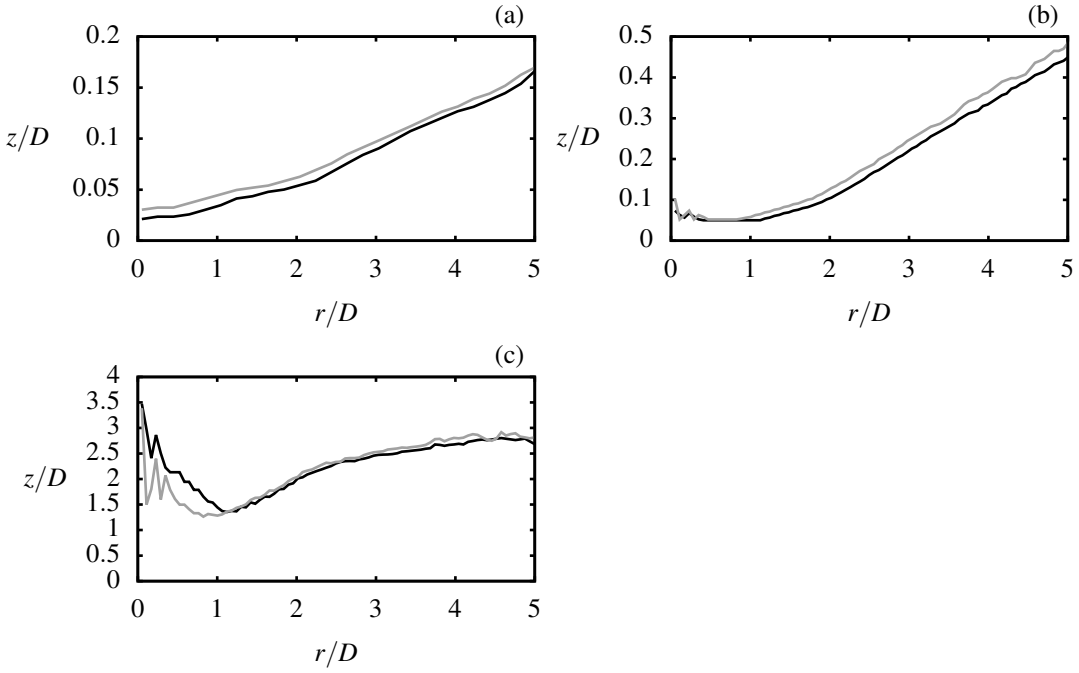

Figure 5. Boundary layer thickness development along the impingement plate. (a) z_m/D; (b) $z_{\theta m}/D$; (c) $z_{\theta m}/z_m$. ———, Smooth wall; ———, rough wall.

$\langle\overline{u_r}\rangle$ is maximum. Similarly, for the temperature, the wall-normal distance $z_{\theta,m}$ at which the mean velocity profile $T_w - \langle\overline{T}\rangle$ is maximum can be taken as a measure of the temperature boundary layer thickness. The development of z_m and $z_{\theta,m}$ for the smooth wall case are shown in figure 4.

A direct comparison between the smooth and rough wall boundary layer thicknesses is reported in figure 5. From the figure, the main effect of surface roughness is that of producing an upward wall-normal shift of the boundary layer thickness at a given radial location.

Figure 5c depicts the ratio between $z_{\theta m}$ and z_m and it shows how the temperature boundary layer is thicker than the velocity boundary layer at any considered radial location. Further, for any radial distance greater than D, the ratio between temperature and velocity boundary layer thicknesses does not seem to be affected by the presence of surface roughness. In fact, in this region of the flow, surface roughness affects both temperature and velocity boundary layer thicknesses individually, but it keeps their ratio almost unchanged. Except for visible fluctuations very close to the jet axis (*i.e.* for $r \leq 0.5D$), $z_{\theta m}$ is constant and equal for all simulated cases for $r < D$ (refer to figure 5b). For larger distances from the jet axis, the temperature boundary layer grows with a linear trend which is markedly visible for $r > 2D$. Within this region, roughness produces a similar outcome to that observed for the velocity boundary layer thickness z_m.

The observation that the temperature boundary layer is thicker compared to the velocity boundary layer supports the fact that impinging jets produce a flow which breaks the Reynolds analogy between momentum and heat transfer along the impingement plate (Woodworth *et al.*, 2023). Close to the jet axis, in the stagnation region of the flow, the Reynolds analogy breaks since a finite wall-heat flux occurs at a vanishing small wall-shear stress. Further downstream, in the wall jet region of the flow, the Reynolds analogy is broken in a favourable way since the wall-heat transfer along the boundary layer decreases at a slower rate compared to the wall-shear stress. We observe that such a behaviour could be connected to the presence of large azimuthal coherent vortical structures that form in the outer layer of the wall jet, in a similar fashion to spanwise coherent vortices that are known to break the Reynolds analogy in fully-developed turbulent channel flows over ridges (Kuwata, 2022).

Sufficiently downstream of the impingement region, the

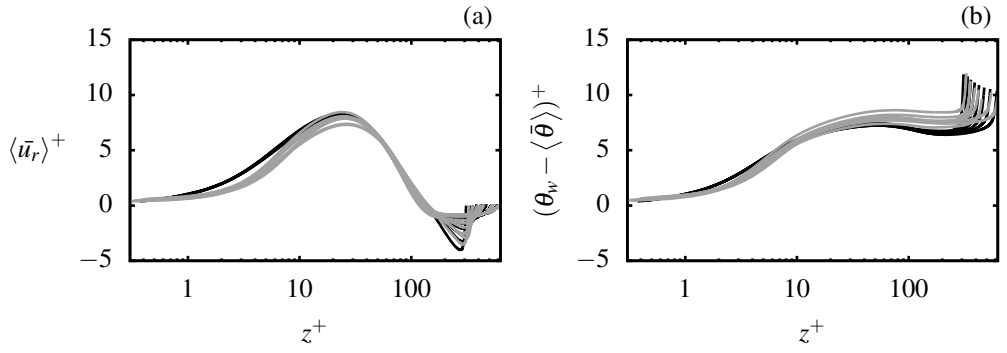

Figure 6. Wall-normal profiles of inner units scaled mean radial velocity (a), and temperature (b) in the range $2.5D < r < 5D$. ———, Smooth wall; ———, rough wall.

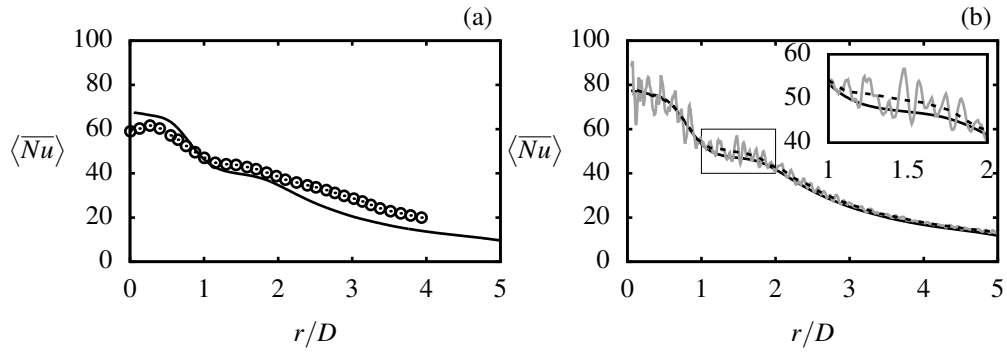

Figure 7. Mean Nusselt number distributions along the impingement plate. (a) Smooth wall case comparison with experimental data, $Pr = 0.7$. Solid line, present DNS; Symbols are from Lee & Lee (1999). (b) Comparison of smooth and rough wall data. ———, smooth wall; ———, rough wall; - - - - - Moving average of rough wall data.

flow exhibit a self similar character, with mean radial velocity and temperature profiles that become similar to each other once they are scaled with the friction velocity $u_\tau = (\tau_w/\rho)^{\frac{1}{2}}$, the viscous length scale $\delta_\nu = \nu/u_\tau$ and the friction temperature $T_\tau = q_w/(\rho c_p u_\tau)$. Here τ_w is the total stress at the wall, ρ is the fluid density, ν is the kinematic viscosity, q_w is the wall-heat flux and c_p is the heat capacity at constant pressure of the fluid. A plus superscript is used to denote viscous units scaled quantities. Figure 6 shows profiles of $\langle \overline{u_r} \rangle^+$ and $(T_w - \langle \overline{T} \rangle)^+$ in the range of radial locations $2.5D < r < 5D$. It is observed that the considered surface roughness only marginally affects the mean velocity and temperature profiles and their self similar character. Yet, the mean profiles of the rough wall case exhibit a visible scatter for $z^+ > 10$. This is due to the fact that, as the flow develops along the boundary layer, the relative size of the roughness changes compared to the viscous length scale and the boundary layer thickness. As such, roughness may impact the flow differently in different regions of the flow. However, the quantification of this effect is rather difficult in the present case due to the lack of sufficient separation of scales which prevents the appearance of well-defined logarithmic region in the mean velocity and temperature profiles. Hence, the effects of surface roughness in terms of roughness functions cannot unambiguously defined (Chung *et al.*, 2021).

The effects of surface roughness on the mean wall-heat transfer distribution along the impingement plate are shown in figure 7(b). In the figure, the mean wall-heat flux is visualized in non-dimensional form in terms of the Nusselt number. Compared to the smooth wall case, large fluctuations characterize the mean Nusselt number distribution of the rough wall case for radial distances $r < 2D$. At larger radii, these fluctuations remain, but their intensity weakens considerably. A net wall-heat transfer increase is only achieved, for the rough wall case, in the range of radial distances $D < r < 2D$, suggesting the favourable effects that surface roughness has on the occurrence of unsteady separation phenomena that lead to the appearance of a secondary peak in the Nusselt number in the same region (Dairay *et al.*, 2015). As a validation of the present numerical framework, the Nusselt number distribution for the smooth wall case is compared with experimental measurements from Lee & Lee (1999) in figure 7(a). A reasonable agreement is observed between present and experimental data, and discrepancies arise due to the difficulties in the numerical simulations to accurately model the boundary conditions of the experiments.

Wall-normal profiles of turbulent kinetic energy in the range of radial distances $D < r < 5D$ are shown in figure 8(a) for the smooth and rough wall cases. Profiles are scaled using the local maximum radial velocity u_m and boundary layer thickness z_m. Similarly to the mean radial velocity (figure 6a), profiles of turbulent kinetic energy exhibit a self-similar character for radial distances $2.5D < r < 5D$, whereas their intensity becomes significantly weaker at smaller radii. At these locations, the turbulent kinetic energy exhibits two distinct peaks: one in the inner region of the wall jet and one in its shear layer. Contrary to the outer peak, the inner one gets quickly damped with increasing radial distance. In fact, as shown in figure 8(b), while the production and dissipation of turbulent kinetic energy are substantially balanced in the outer region of the wall jet, an imbalance between dissipation and production exists in the inner region which favors the dissipation of turbulent kinetic energy.

This feature seems to be unaltered for the rough wall case, even though a slight increase in the production of turbulent ki-

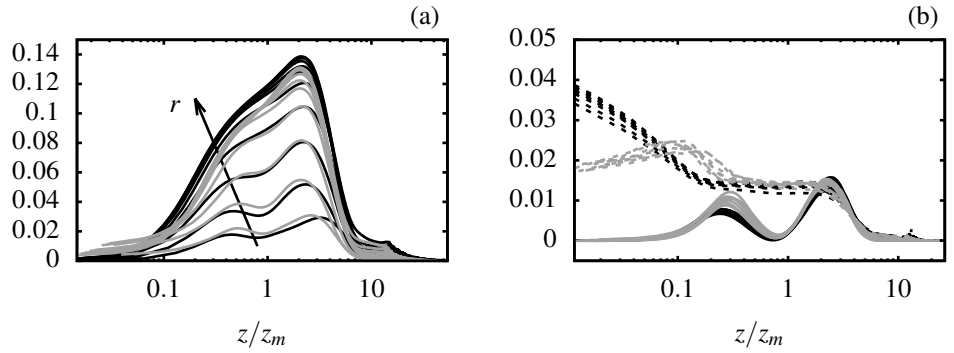

Figure 8. Wall-normal profiles of outer units scaled turbulent kinetic energy (a), and production and dissipation of turbulent kinetic energy (b). Black lines represent the smooth wall case, whereas grey lines are used for the rough wall case. In panel (b), solid and dashed lines depict, respectively, the production and the dissipation of turbulent kinetic energy.

netic energy is observed in the inner region. The shear-driven turbulent kinetic energy production mechanism in the inner region of the wall jet appears to be weak and, correspondingly, surface roughness only marginally affects flow properties in this region. The proposed analysis will further explore this scenario and focus on the development region of the wall jet where surface roughness shows a net effect on integral properties of the flow (*i.e.* $D < r < 2D$).

CONCLUSIONS

This work presents DNS results of turbulent circular jets impinging on smooth and rough walls where the jet is produced by a fully-developed turbulent pipe flow at a bulk Reynolds number $Re = 5300$. The latter was defined using the mean bulk velocity in the pipe and its diameter. The investigated nozzle-to-plate distance was set to be twice the diameter of the pipe used to produce the turbulent jet. This particular choice is known in the literature to produce a localized enhancement of the mean wall-heat flux due to the interaction of vortical structures with the wall (Dairay *et al.*, 2015).

The rough surface selected for the present study was an in-plane homogeneous topography having a Gaussian PDF with 99% width of the confidence interval $k_{99} = 0.05D$ and a power spectrum whose shortest resolved wave-length was $\lambda_{min} = 0.04D$.

The jet impingement produces a complex flow which consists of a free-jet, a stagnation, and a wall jet region. Surface roughness produces a noticeable increase in the boundary layer thicknesses of the velocity and temperature fields, everywhere along the impingement plate. Interestingly, the flow exhibits a favourable breaking of the Reynolds analogy between heat and momentum transfer which does not appear to be influenced by the investigated rough surface. It is pointed out that the breaking of the Reynolds analogy could be linked to the presence of large toroidal coherent vortical structures which originate in the shear-layer of the wall jet, similarly to what is seen with Kelvin-Helmholtz instabilities which occur over streamwise-aligned ridges (Kuwata, 2022).

The considered surface roughness does not significantly modify the mean velocity and temperature profiles sampled at various radial locations. Viscous units scaling of such profiles shows that their self-similar character is only marginally affected by the presence of the roughness. Further, the assessment of the mean radial distribution of the wall-heat flux, in terms of Nusselt number, shows small changes between the smooth and rough wall cases.

An analysis of the turbulence production and dissipation profiles at several radial locations revealed that the inner layer of the wall jet is dominated by the dissipation of turbulent kinetic energy, whereas, in the outer layer, turbulence production and dissipation match each other. In light of these observations, it is suggested that the near-wall turbulence is sustained at the expenses of the outer layer flow through redistribution mechanisms. This scenario appears not to be affected by the small scales that characterize the considered roughness topography, suggesting that such production and redistribution of turbulence fluctuations phenomena are associated with relatively much larger flow structures.

ACKNOWLEDGEMENTS

We greatly acknowledge the support by the German Research Foundation (DFG) under the Collaborative Research Centre TRR150 (project number 237267381). The simulations presented in this work were performed on the HPE Apollo (Hawk) supercomputer at the High Performance Computing Center Stuttgart (HLRS) under the grant number zzz44198.

REFERENCES

Chung, D., Hutchins, N., Schultz, M. P. & Flack, K. A. 2021 Predicting the drag of rough surfaces. *Annual Review of Fluid Mech.* **53** (1), 439–471.

Dairay, T., Fortuné, V., Lamballais, E. & Brizzi, L.-E. 2015 Direct numerical simulation of a turbulent jet impinging on a heated wall. *J. of Fluid Mech.* **764**, 362–394.

Dong, S. 2015 A convective-like energy-stable open boundary condition for simulations of incompressible flows. *J. Comput. Phys.* **302**, 300 – 328.

Ekkad, S.V. & Singh, P. 2021 A Modern Review on Jet Impingement Heat Transfer Methods. *J. of Heat Transfer* **143** (6).

Fisher, P.F., Lottes, J.W. & Kerkemeier, S.G. 2008-2020 NEK5000 Version 19.0. Argonne National Laboratory, Illinois.

Jambunathan, K., Lai, E., Moss, M.A. & Button, B.L. 1992 A review of heat transfer data for single circular jet impingement. *Int. J. of Heat and Fluid Flow* **13** (2), 106–115.

Kuwata, Y. 2022 Dissimilar turbulent heat transfer enhancement by kelvin–helmholtz rollers over high-aspect-ratio longitudinal ribs. *Journal of Fluid Mechanics* **952**, A21.

Lee, J. & Lee, S. J. 1999 Stagnation region heat transfer of a turbulent axisymmetric jet impingement. *Exp. Heat Transfer* **12** (2), 137–156.

Liu, X., Xie, Z. & Dong, S. 2020 On a simple and effective thermal open boundary condition for convective heat transfer problems. *Int. J. of Heat and Mass Transfer* **151**, 119355.

Maday, Y. & Patera, A.T. 1989 Spectral element methods for the incompressible Navier-Stokes equations. In *State of the art surveys on computational mechanics ASME*, pp. 71–143.

Pèrez-Ràfols, F. & Almqvist, A. 2019 Generating randomly rough surfaces with given height probability distribution and power spectrum. *Tribology Int.* **131**, 591–604.

Secchi, F., Gatti, D. & Frohnapfel, B. 2023 The wall-jet region of a turbulent jet impinging on smooth and rough plates. *Flow, Turb. and Comb.* **110** (2).

Secchi, F., Häber, T., Gatti, D., Schulz, S., Trimis, D., Suntz, R. & Frohnapfel, B. 2022 Turbulent impinging jets on rough surfaces. *GAMM-Mitteilungen* p. e202200005.

Woodworth, A. D., M., Salazar D. & T., Liu 2023 Heat transfer and skin friction: Beyond the reynolds analogy. *Int. J. of Heat and Mass Transfer* **206**, 123960.

Wu, W., Banyassady, R. & Piomelli, U. 2016 Large-eddy simulation of impinging jets on smooth and rough surfaces. *J. of Turbulence* **17** (9), 847–869.